Green Chemistry



PAPER

View Article Online
View Journal



Cite this: DOI: 10.1039/d0gc01412e

Utilizing hydrogen underpotential deposition in CO reduction for highly selective formaldehyde production under ambient conditions†

Libo Yao,‡ Yanbo Pan,‡ Xiaochen Shen, Dezhen Wu, Abdulaziz Bentalib and Zhenmeng Peng

*

Formaldehyde is an essential building block for hundreds of chemicals and a promising liquid organic hydrogen carrier (LOHC), yet its indirect energy-intensive synthesis process prohibits it from playing a more significant role. Here we report a direct CO reduction to formaldehyde (CORTF) process that utilizes hydrogen underpotential deposition to overcome the thermodynamic barrier and the scaling relationship restriction. This is the first time that this reaction has been realized under ambient conditions. Using molybdenum phosphide as a catalyst, formaldehyde was produced with nearly a 100% faradaic efficiency in aqueous KOH solution, with its formation rate being one order of magnitude higher compared with the state-of-the-art thermal catalysis approach. Simultaneous tuning of the current density and reaction temperature led to a more selective and productive formaldehyde synthesis, indicating the electrochemical and thermal duality of this reaction. DFT calculations revealed that the desorption of the *H2CO intermediate likely served as the rate-limiting step, and the participation of H₂O made the reaction thermodynamically favorable. Furthermore, a full-cell reaction set-up was demonstrated with CO hydrogenation to HCHO achieved without any energy input, which fully realized the spontaneous potential of the reaction. Our study shows the feasibility of combining thermal and electrochemical approaches for realizing the thermodynamics and for scaling relationship-confined reactions, which could serve as a new strategy in future reaction design.

Received 22nd April 2020, Accepted 20th June 2020 DOI: 10.1039/d0gc01412e

rsc.li/greenchem

Introduction

The rise of the hydrogen economy and fuel cell technologies have stimulated extensive research efforts in the associated fields, among which hydrogen storage remains a challenging topic. With a hydrogen storage capacity of 8.3 wt% in its hydrated form, formaldehyde (HCHO) holds theoretical promise as an excellent liquid organic hydrogen carrier (LOHC), which releases H₂ *via* decomposition and can be regenerated *via* hydrogenation. It is also advantageous compared to other LOHC candidates, like methanol and formic acid, However, HCHO is the least investigated among the three chemicals that have been studied for LOHC application in previous studies, which suffered from the harsh reaction conditions required for HCHO synthesis causing a high

Department of Chemical and Biomolecular Engineering, The University of Akron, Akron, OH 44325, USA. E-mail: zpeng@uakron.edu

energy cost.^{13–15} In practice, HCHO is produced by methanol as a precursor following the so-called Formox process,¹⁶ which partially oxidizes methanol to HCHO above 400 °C.¹⁷ Considering that methanol is typically synthesized from syngas at an elevated temperature and high pressure,¹⁸ the overall HCHO production process is a high energy-consumption process, which restricts its use for LOHC application. Besides, HCHO is an important precursor for synthesizing many more complex chemicals, like resins, 1,4-butanediol, polyols, and so on, which demand an annual HCHO production of over 50 million tons.^{19–21} Consequently, development of a new, cost-effective method for HCHO synthesis would not only decrease the production cost for its many uses but also enable its application as a LOHC for hydrogen-storage research.

From a thermodynamic point of view, gaseous HCHO can be directly synthesized from syngas via CO hydrogenation, which would skip the energy intensive methanol synthesis and the Formox steps. The reaction has a positive ΔG° value in the gas phase (eqn (1)), making it barely possible to take place under standard conditions.²² However, ΔG° turns slightly negative when the reaction occurs in an aqueous phase (eqn

 $[\]dagger\, Electronic$ supplementary information (ESI) available. See DOI: 10.1039/d0gc01412e

[‡]These authors contributed equally to this article.

(2)), benefiting from the contribution of the heat released during HCHO solvation. This offers an opportunity to realize aqueous HCHO synthesis from direct CO hydrogenation.¹¹

$$CO_{(g)} + H_{2(g)} \rightarrow HCHO_{(g)} \quad \Delta \textit{G}^{\circ} = +34.6 \text{ kJ mol}^{-1} \qquad (1)$$

$$\mathrm{CO_{(g)}} + \mathrm{H_{2(g)}} + \mathrm{H_{2}O_{(aq)}} \rightarrow \mathrm{HCHO} \cdot \mathrm{H_{2}O_{(aq)}}$$

$$\Delta G^{\mathrm{o}} = -7.1 \, \mathrm{kJ} \, \mathrm{mol}^{-1} \qquad (2)$$

As a matter of fact, Tanksale et al. demonstrated a successful case by thermally catalyzing CO hydrogenation using Pd-Ni and Ru-Ni/Al₂O₃ catalysts in aqueous solution, 22,23 with a small amount of HCHO obtained proving the viability of this route. However, the achieved HCHO generation rate was low, being less than 3 mg $(g_{cat} h)^{-1}$ even when using the best performing catalyst and under a harsh condition of high pressure (20-120 bar), which is far from satisfactory in terms of potential industrial application. The slow reaction kinetics can be explained in terms of the discovered scaling relationship in catalysis. 24-26 CO molecules chemisorb more strongly to catalysts than H₂ does in a generic trend. This leads to the active sites being dominantly occupied by CO with few active sites available for H2 molecules to adsorb and dissociate, which consequently inhibits the reaction. From this perspective, it would be challenging to realize efficient CO hydrogenation to aqueous HCHO, unless there are means to break the scaling relationship to achieve a more balanced H₂ adsorption.

Electrocatalysis has received significant attention in reducing CO2 to energy fuels in the aqueous phase under mild conditions. In comparison, CO electrochemical reduction has been less intensively investigated. 27-29 Instead, more research focus has been put on tandem reactions starting from CO₂, with the aim to establish a CO2-CO-chemical network.30-32 Similar to CO₂ electrochemical reduction, Cu-based materials are mainly used in CO electrochemical reduction, where they lead to the generation of different products, including hydrocarbons,34,35 methane, 30,33 alcohols29,36 acetates.37-39 To the best of our knowledge, no direct HCHO synthesis via CO electrochemical reduction has yet been achieved, which indicates that the catalysis mechanism of Cubased materials doesn't favor HCHO formation. A new catalysis mechanism would be required to realize the electrochemical synthesis of aqueous HCHO.

Herein, we report a new synthesis strategy that combines thermal CO reduction catalysis with hydrogen underpotential deposition, which is a pre-step for the hydrogen evolution reaction (HER), to reduce CO to aqueous HCHO. Direct, selective CO reduction to formaldehyde (CORTF) was achieved under ambient conditions using a molybdenum phosphide (MoP) catalyst, which has been previously studied as an efficient catalyst in the hydrogen evolution reaction (HER) but it is known to have a poor CO adsorption capability. We report that formaldehyde could be generated with 100% selectivity at room temperature *via* a combinational utilization of electrochemical and thermal reaction mechanisms. The CORTF process improved the formaldehyde formation rate to one order of

magnitude higher than the previous thermal catalysis method. 22,23 We further demonstrated spontaneous, selective HCHO synthesis at room temperature in a full-cell, with CO fed to one electrode for CORTF and $\rm H_2$ fed to the other for the hydrogen oxidation reaction. Effective aqueous HCHO production was thus realized without any energy input, confirming the great potential of this new CORTF method.

Experimental

Catalyst preparation

Molybdenum phosphide (MoP) was prepared by a temperature-programmed reduction (TPR) method. The molybdenum precursor, ammonium molybdate tetrahydrate, $(NH_4)_6Mo_7O_{24}\cdot 4H_2O$, and the phosphorus source, ammonium phosphate dibasic, $(NH_4)_2HPO_4$, were dissolved in DI water in an equimolar amount in terms of Mo and P. The mixture was stirred and dried overnight at 80 °C, followed by calcination at 500 °C for 4 h. The resultant sample then underwent TPR with flowing H_2 (50 ml min⁻¹). The procedures included ramping to 350 °C at a rate of 5 °C min⁻¹, followed by increasing the temperature to 650 °C at 2 °C min⁻¹ and holding at this temperature for 2 h. The sample was cooled down to room temperature and then purged with Ar for another 1 h before being collected.

Catalyst characterization

The as-prepared and spent MoP samples were characterized by transmission electron microscopy (TEM) using a JEOL JEM-1230 microscope with an accelerating voltage of 120 kV. High-resolution TEM (HRTEM) images were taken using an FEI Tecnai G2 F20 microscope operated at 200 kV. The powder X-Ray diffraction (PXRD) patterns were recorded on a Rigaku Ultima IV multipurpose X-ray diffraction system with CuKα radiation source. The XPS spectra were obtained with a PHI 5000 Versaprobe II X-Ray photoelectron spectrometer. SEM images and EDX mapping were obtained on a Tescan LYRA3 machine with a working voltage of 10 kV for SEM and 20 kV for the mapping mode. In situ diffuse reflectance infrared Fourier transform spectroscopy (DRIFTS) experiments were conducted with a Nicolet 6700 FTIR spectrometer equipped with the Harrick Praying Mantis DRIFTS accessory. The spectra were recorded by collecting 64 scans at a resolution of 4 cm^{-1} .

Electrode preparation and electrochemical measurements

The electrochemical measurements were conducted on a Gamry Reference 600+ potentiostat in an undivided electrochemical cell, which included a three-electrode configuration. MoP deposited on carbon cloth (MoP/CC) was used as the working electrode (WE), while Ag/AgCl and Pt wire were used as the reference electrode (RE) and counter electrode (CE), respectively. For the preparation of WE, MoP ink was first made by dispersing 1 mg MoP powder in 0.5 mL isopropanol containing 2 µL Nafion as a binding agent. After sonification,

the ink was uniformly dispersed on a 2 cm \times 1 cm hydrophilic carbon cloth. In most experiments, 0.5 M KOH was used as the default electrolyte unless otherwise noted. All the potentials in this work were converted to those *versus* the reversible hydrogen electrode (RHE) by calibration in 0.5 M KOH, with the transformation shown in eqn (3):

$$E(RHE) = E(Ag/AgCl) + 0.906$$
 (3)

Polarization curves were obtained under linear sweep voltammetry at a 10 mV s^{-1} scan rate. Electrochemical impedance spectroscopy (EIS) was carried out in the frequency range of $100\,000$ to 0.01 Hz under the amplitude of 10 mV.

The half-cell CO electrochemical reduction tests were performed with continuous feeding of CO gas. Prior to each run, CO was bubbled in to the solution for 1 h at a flow rate of 20 ml min⁻¹ for saturation, and it was continuously fed at the same rate during the measurement.

Full-cell CO reduction was conducted in a H-type 2-compartment cell with a two-electrode configuration in 0.5 M KOH electrolyte. A FUMASEP-FAB-130 anion exchange membrane was placed between the two compartments. The MoP/CC electrode was placed in the cathodic compartment with 20 ml min $^{-1}$ CO feed, while the Pt electrode was placed in the anodic one with 20 ml min $^{-1}$ H $_2$ continuously flowed through. The cathodic, anodic, and overall reactions are shown in the following:

Cathode:

$$CO + 3H_2O + 2e^- \rightarrow HCHO \cdot H_2O + 2OH^- \tag{4}$$

Anode:

$$H_2 + 2OH^- \rightarrow 2H_2O + 2e^-$$
 (5)

Overall:

$$CO + H_2 + H_2O \rightarrow HCHO \cdot H_2O$$
 (6)

Product analysis and quantification

The gas products from the reaction were analyzed through an Agilent 6890 GC-MSD system, and the liquid products were analyzed by ¹H-NMR using a Bruker AVIII 750 MHz NMR spectrometer. Typically, 500 µL of collected electrolyte after the reaction was mixed with 100 µL D₂O. The ¹H spectrum was measured with water suppression using a pre-saturation method. In the spectra from the GC-MS and ¹H-NMR (Fig. S1 and S2†), no carbonaceous gaseous products or liquid products other than formaldehyde were detected under our reaction conditions (50 µA cm⁻²). Therefore, the products could be considered to include only H2 and HCHO, and the calculation of the faradaic efficiency (FE) could be performed based on formaldehyde formation. Formaldehyde was quantified by an adapted acetylacetone method. 42 To start with, 0.25% (v/v) acetylacetone solution was prepared by dissolving 25 g ammonium acetate, 3 ml acetic acid, and 0.25 ml acetylacetone in DI water and the volume of the solution was fixed at 100 ml. Then a series of formaldehyde standard solutions (0,

0.083, 0.333, 0.833, 1.667, 2.5, and 2.917 μg ml⁻¹) were prepared. Next, 5 ml of each of the standard solutions with 1 ml 0.25% acetylacetone solution were mixed and put in a boiling water bath for 3 min. After cooling down to room temperature, the solution was transferred to a Shimadzu UV-2600 spectrophotometer for the detection of absorbance from the 800-190 nm wavelength. A working curve (Fig. S4†) was constructed by building the relationship between the absorbance at 413 nm (Fig. S3†) and concentration of the standard solutions, and it turned out to be perfectly linear. The curve was therefore used for the quantification of formaldehyde for all the samples obtained in this work. The faradaic efficiency of HCHO (FE_{HCHO}) could be calculated using FE_{HCHO} = $(nF \times V)/(I$ \times t) \times 100, where n is the number of electrons being transferred, F is Faraday's constant, x is the concentration of HCHO, V is the volume of electrolyte, I is the current, and t is the reaction time.

DFT calculations

DFT calculations were performed using the Quantum ESPRESSO package.43 Generalized gradient approximation (GGA) and the Perdew-Burke-Ernzerhof (PBE) with projectoraugmented wave (PAW) sets from PSlibrary 0.3.1 were used to carry out the structure relaxation and energy calculations.44 The bulk lattice of MoP was optimized prior to the cleavage of the (001) surface. The slab model of MoP was constructed using a p (3×3) unit cell with six layers of close-packed (001) surfaces, which were separated by a vacuum layer of 20 Å in the direction perpendicular to the surface. A plane wave basis set was used with a cutoff energy of 450 eV with a density cutoff of 4500 eV and a Monkhorst-Pack k-point mesh of 5 × 5 × 1, and the Fermi-level smearing was set at 0.1 eV. The bottom four layers of atoms were held fixed in their bulk positions, while the top two layers of atoms and all the adsorbate degrees of freedom were allowed to relax.

Results and discussion

Characterization of the MoP catalyst

The MoP synthesis followed a widely adopted temperature programmed reduction method reported in a previous study. 41 The XRD pattern indicated a pure hexagonal structure (ICDD 03-065-6487) with a space group belonging to $P\bar{6}m2$ (Fig. S5†). HRTEM characterization exhibited well-arrayed (001) and (101) planes with d-spacings of 0.32 and 0.21 nm, respectively (Fig. S6a†). A thin amorphous layer was observable on the MoP surface, which suggested slight surface oxidation caused by sample exposure to the atmosphere. 45 SEM imaging and EDX mapping showed an even distribution of Mo and P elements throughout the sample (Fig. S6b-d†), which was consistent with the XRD data and confirmed a uniform MoP phase. XPS spectroscopy of Mo 3d and P 2p bands showed dominant signals assignable to the MoP phase (Fig. S7†). The Mo 3d spectra exhibited two minor deconvoluted peaks at 231.4 and 234.3 eV, which were assignable to Mo⁶⁺ as a result of slight

surface oxidation due to exposure to air, which was in good agreement with previous reports.

Experimental evaluation of CO reduction to formaldehyde

The first step in achieving CO reduction to formaldehyde (CORTF) is finding an appropriate electrolyte. Fig. 1a shows the linear sweep voltammetry (LSV) curves of MoP in CO-saturated acidic (0.5 M H₂SO₄, pH = 0.6), neutral (0.5 M Na₂SO₄, pH = 6.7), and alkaline (0.5 M KOH, pH = 13.2) media. The currents were corrected with the ohmic resistance (R_s , Table S1†), fitted with an equivalent circuit obtained from the electrochemical impedance spectroscopy results (Fig. S9†). For comparison purposes, LSV curves were also obtained under a CO absence condition, which corresponded to the HER (Fig. S10†). In both cases, the catalytic activity of MoP represented by the current density followed the same order of $H_2SO_4 > KOH \gg Na_2SO_4$. Tafel plots were subsequently derived from the LSV curves (Fig. S11†). Nearly identical values and Tafel slopes, namely 92.0 mV dec⁻¹ in the presence of CO versus 93.5 mV dec⁻¹ in the absence of CO, were obtained in H₂SO₄, suggesting the activity accounted predominantly for the HER but little CO reduction. Interestingly in KOH electrolyte, the Tafel slope changed significantly from 94.4 to 119.3 mV dec⁻¹ after CO was introduced, suggesting an alteration in the reaction kinetics in the presence of CO and implying possible CORTF occurrence. A similar phenomenon was also observed in neutral electrolyte; however, the overall activity was too low to be considered. The CORTF reaction was confirmed by analyzing the liquid and gas products collected

at -5 mA cm⁻² with GC-MS and ¹H-NMR (Fig. S1 and S2†), which found HCHO as the only product besides H₂. Quantitative analyses showed little HCHO was produced in acidic electrolyte but considerable HCHO formation occurred in alkaline solution (Fig. 1b). This finding indicates HCHO could indeed be produced *via* CORTF in an appropriate electrolyte even under ambient conditions. It needs to be noted that the HCHO faradaic efficiency (FE_{HCHO}) was calculated to be only 0.52% under the specific testing condition, suggesting a need for performance optimization.

By carefully comparing with the LSV curve obtained in Arprotected 0.5 M KOH, we observed that the current density was lower by about -0.2 V but higher above this potential when CO was present (Fig. 1c). This revealed that the CORTF contribution to the overall current density was more significant before the onset potential, where the hydrogen underpotential deposition (HUPD) occurs. This is a good indication that the deposited hydrogen was combined with CO for formaldehyde production. Fig. 1d shows the difference between the two Tafel plots, which can yield more insights. The Tafel plot with CO shows two linear sections, which intersected at about -0.2 V in terms of the potential and about -0.5 in terms of $\log |j|$, which corresponds to a low current density of -0.3 mA cm⁻². The plot exhibits an abnormally high Tafel slope of 895 mV dec⁻¹ in the upper potential range, i.e., the lower current density range. This value is distinct from 119 mV dec⁻¹ in the lower potential range where the HER dominates, implying a possible dominance by the CORTF reaction in this regime.

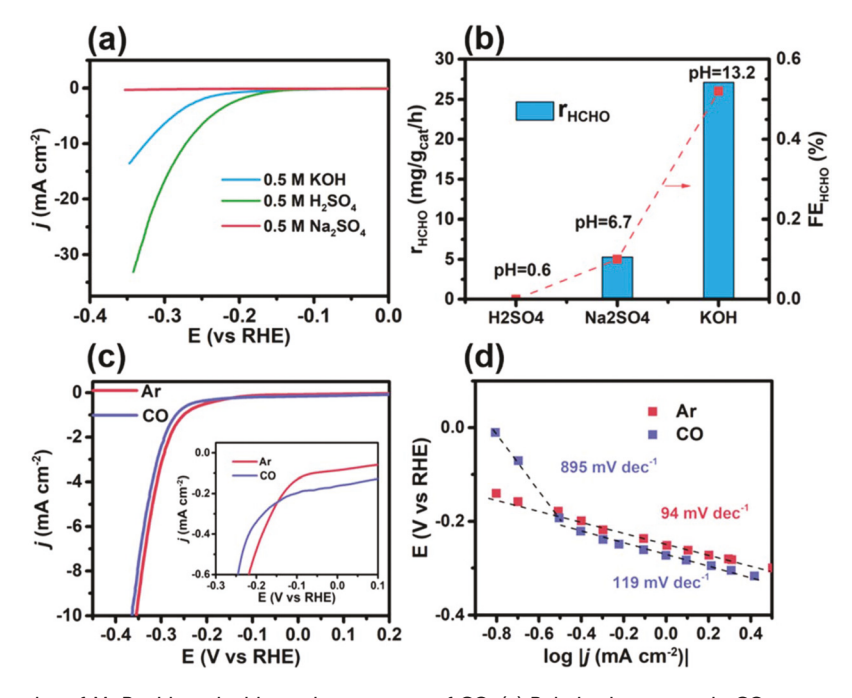


Fig. 1 Electrocatalytic properties of MoP with and without the presence of CO. (a) Polarization curves in CO-saturated acidic (0.5 M H_2SO_4 , pH = 0.6), neutral (0.5 M Na_2SO_4 , pH = 6.7), and alkaline (0.5 M KOH, pH = 13.2) electrolytes. (b) Effect of the electrolyte on formaldehyde formation at -5 mA cm⁻². (c) Comparison of the polarization curves and the zoom-in curves from -0.2 to 0.1 V (inset) in 0.5 M KOH electrolyte with and without CO. (d) Tafel plots obtained from the polarization curves in (c).

Green Chemistry Paper

As shown in our in situ DRIFTS experiment (Fig. S12†) as well as in previous studies, 41 it is known that MoP barely chemisorbs CO. CORTF likely resulted from the reaction between dissolved CO and in situ-generated *H species on MoP active sites. In other words, there exists a competition relationship between CORTF and HER (Fig. 2). Sharing the same hydrogen deposition step that generates *H species, the product preference is dependent on the potential, as a higher overpotential explicitly triggers HER, while CORTF is more significant within the underpotential range (<-0.2 V). The HCHO generation rate (r_{HCHO}) and FE_{HCHO} as well as their dependence on the testing conditions were thus carefully examined in the lower current density range. There was a clear trend that with a decrease in current density, rHCHO decreases monotonously while FE_{HCHO} keeps on increasing (Fig. 3a), with FE_{HCHO}

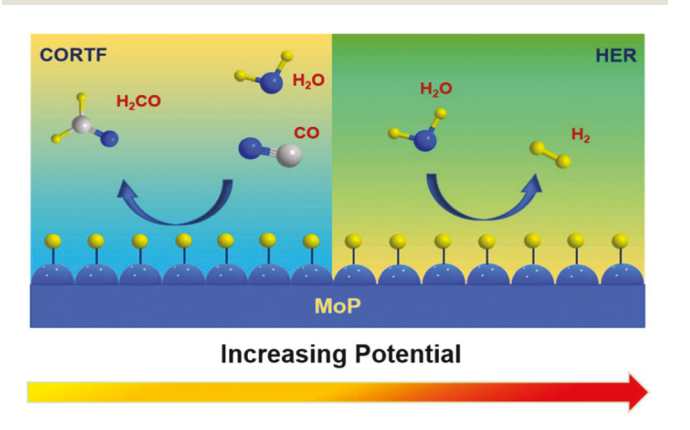


Fig. 2 Schematic representation of competitive CORTF and HER pathways.

reaching 96.6% at $-5 \mu A \text{ cm}^{-2}$. This finding reveals that HCHO can be more selectively produced at a lower current density, i.e., at a more positive potential. The alteration in product distribution between HCHO and H2, considering the HER kinetics, is purely potential dependent, implying the CORTF kinetics does not simply rely on the electrochemical potential but also some other factors. This was confirmed by examination of the temperature effect on the reaction kinetics and on the selectivity by keeping the electrode potential unchanged (E =-30 mV, Fig. 3b). Both the $r_{\rm HCHO}$ and ${\rm FE}_{\rm HCHO}$ increased with temperature, suggesting CORTF as a "hybrid" reaction with the kinetics being influenced by not only the electrochemical potential but also the thermochemistry. An apparent activation energy of 17.1 kJ mol⁻¹ was determined for CORTF from the Arrhenius plot (Fig. S13†). The temperature effect showed the same trend when the current density was fixed at -250 and $-50 \mu A \text{ cm}^{-2}$ (Fig. S14†). The exception appeared at $-5 \mu A$ cm $^{-2}$, where both r_{HCHO} and FE_{HCHO} became nearly independent of the temperature with FE_{HCHO} approaching 100%. At this low current density, the CORTF rate would likely be restricted by the *H generation rate but not the following steps that are influenced by temperature. By simultaneously tuning the current and temperature, HCHO could be produced at a rate of over 30 mg $(g_{cat} h)^{-1}$, with more than a 50% faradaic efficiency (Fig. S14b†). This activity is over one order of magnitude higher than that of the state-of-the-art thermal catalysis approach (Table S2†). The electrolyte concentration effect on the CORTF properties was also examined (Fig. 3c and Fig. S15†). An increase in the KOH concentration led to an enhancement in r_{HCHO} . It is well known that a higher electrolyte concentration can substantially increase the HER intrinsic activity, leading to a more positive onset potential and lower

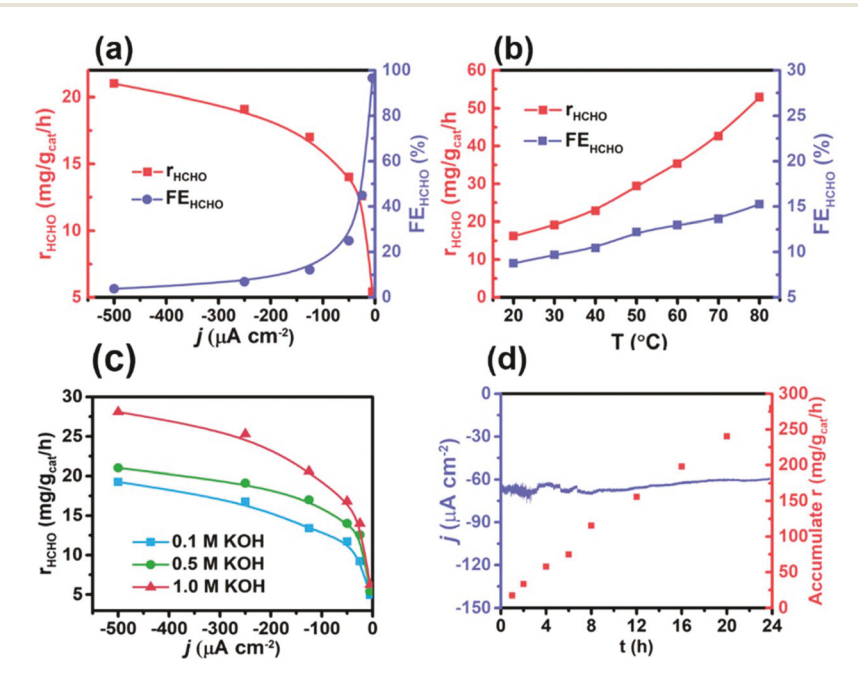


Fig. 3 CORTF properties on MoP and the influencing factors. (a) Measured r_{HCHO} and FE_{HCHO} as a function of the current density. (b) Temperature effect on r_{HCHO} and FE_{HCHO} obtained at E = -30 mV (vs. RHE). (c) Effect of the electrolyte concentration on r_{HCHO} . (d) Stability test at 0.2 V vs. RHE.

Paper

Tafel slope. 46,47 Such an enhancement would contribute to more efficient hydrogen deposition and subsequent CO reduction.

The durability test at 0.2 V vs. RHE, where CORTF dominates, showed a minor decrease of less than 20 μA cm⁻² in the current density within 24 h, suggesting good stability of the MoP catalyst (Fig. 3d). The slight reaction rate decrease could be related to a reduced CO mass-transfer efficiency caused by a mismatch between the continuous CO_{aq} consumption and under-compensation due to a low solubility (Fig. S16†). Based on measurements of the accumulative HCHO production amount after different periods of time, it could be deduced that the CORTF reaction rate was relatively faster at the very beginning and then remained steady till completion of the stability test. It is worth mentioning that the measured electrode potential became positive when the current density was below -250 μA cm⁻² (Fig. S17†), which could be attributed to a more positive CORTF potential than with the HER induced by the presence of CO (Fig. S18†). XRD characterizations of the MoP catalyst after the stability test showed no observable differences in the fresh sample, confirming its structural stability (Fig. S8†).

Proposed reaction pathway and DFT calculations

Density functional theory (DFT) simulations of both the CORTF and HER pathways were conducted to gain more insights into the reaction mechanism and properties (Fig. S19†). Fig. 4 presents the calculated Gibbs free energy diagram for the two reactions on Mo-terminated MoP (001) surface at E = 0 V. Details on the structure and energy information of the surface intermediates are summarized in Fig. S20 and Table S3,† respectively. The two reactions share a same initial step (step 1), i.e., the Volmer step, in which *H is generated on the MoP surface. The generated *H could follow the Heyrovsky mechanism to further electrochemically react, which leads to HER and thus H2 formation. Alternatively, *H could react with free molecular CO_{aq} to form *HCO (step 2), which involves no electron transfer and is hence a non-galvanic process. *HCO would be further hydrogenated to *H2CO (step 3), followed by desorption to form HCHO (step 4), and

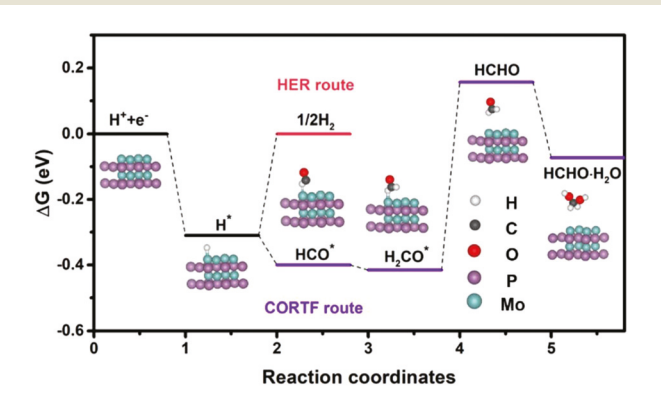


Fig. 4 Gibbs free energy diagram of DFT-simulated CORTF and HER pathways at E = 0 V.

then solvation to form dissolved HCHO (step 5). Thus the CORTF reaction pathway combines both galvanic and non-galvanic steps, which makes it subject to the influence of both electrochemical and thermal factors. The most energy demanding step for CORTF was found to be *HCHO desorption, which is likely the rate-limiting step. Moreover, the result agrees with the reaction thermodynamics, which states that CO reduction to gas-phase HCHO has a positive ΔG value of 0.16 eV. The solvation effect due to HCHO dissolution in water turns the overall reaction into a spontaneous process (ΔG = -0.06 eV).

Spontaneous CO hydrogenation to formaldehyde in the fullcell configuration

Based on the finding that MoP can catalyze CORTF with high selectivity at E > 0 V, spontaneous CO hydrogenation to HCHO was demonstrated in a full-cell configuration. Fig. 5a and Fig. S21† show a schematic and photograph of a simple H-type two-compartment cell set-up, which consisted of carbon cloth-

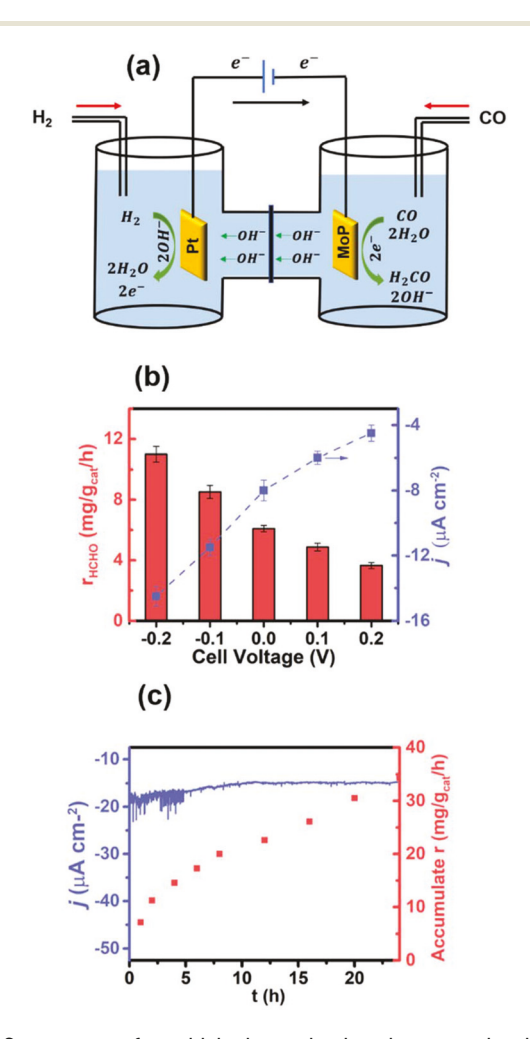


Fig. 5 Spontaneous formaldehyde production demonstration in a full cell. (a) Graphic representation of the full-cell configuration. (b) Formaldehyde formation rate as a function of cell voltage. (c) Cell durability test at 0 V cell voltage.

Green Chemistry Paper

supported MoP as the cathode, Pt wire as the anode, and aqueous KOH as the electrolyte. An anion-exchange membrane was employed between the two compartments, which allowed hydroxyl ion migration across the membrane but prevented the crossover of gases. CO was fed to the cathode compartment where CORTF occurs, leading to solvated HCHO formation (eqn (4)), and H2 was simultaneously fed to the anode compartment, where hydrogen oxidation reaction occurs (eqn (5)). Fig. 5b shows the full-cell testing results with different voltage loads. Interestingly even under zero cell voltage condition, HCHO was still produced at a rate of 6.1 mg $(g_{cat} h)^{-1}$, indicating the spontaneity characteristic of the reaction. Thus direct HCHO synthesis from CO hydrogenation could be realized without any energy input under ambient conditions with a full electrochemical cell setup. A faster HCHO formation rate was yielded with a more negative cell voltage, which was consistent with the observed potential dependency of the CORTF activity on MoP. It should be noted that the achieved HCHO formation rate under the full-cell condition was lower than that under the half-cell condition, which was attributed to the considerable internal resistance of the anion exchange membrane and the simple cell setup without optimization. The durability of the full-cell for HCHO production was evaluated at 0 V for 24 h (Fig. 5c). HCHO was continuously produced under the testing conditions as evidenced by its measured accumulated amount over the course of the reaction time. Less than 5 μA cm⁻² decay in the current density was witnessed during the 24 h test, indicating good cell durability.

Conclusions

In summary, we reported a new strategy for realizing direct CO reduction to formaldehyde (CORTF) under ambient conditions by means of combining electrochemical and thermal approaches. For the first time, formaldehyde was successfully produced at room temperature and ambient pressure in an aqueous medium. The experimental results and DFT simulations suggest the reaction was initiated by means of "sharing" the hydrogen underpotential deposition (HUPD) with HER, where H_{ad} was in situ electrocatalytically generated on MoP. This broke down the scaling relationship restriction in thermal CO reduction catalysis, wherein H2 dissociative adsorption to generate Had is strongly inhibited due to the always stronger CO adsorption, which poisons the catalyst. CO then reacted with Had following the thermal catalysis pathway, leading to formaldehyde formation. Up to 100% CORTF faradaic efficiency was achieved by controlling the positive catalyst potential to inhibit HER. By tuning the electrochemical and thermal condition parameters, an HCHO production rate as high as 31 mg $(g_{cat} h)^{-1}$ was obtained, which was one order of magnitude higher than that from the previously reported thermal catalysis method $(2-3 \text{ mg } (g_{cat} \text{ h})^{-1})$. More importantly, spontaneous CO hydrogenation to formaldehyde was realized by demonstrating the overall reaction in a full-cell. Continuous formaldehyde production was observed by feeding CO and H₂ to the cathode and the anode without applying any cell voltage. The concept of hybridizing electrocatalysis and thermal catalysis for overcoming the thermodynamic barrier can not only realize successful direct spontaneous formal-dehyde synthesis under ambient conditions, but also is likely extendable to a wide range of thermodynamically and kinetically confined reactions.

Conflicts of interest

There are no conflicts to declare.

Acknowledgements

We acknowledge the financial support of this work by National Science Foundation (1665265).

The authors are grateful to Dr Andrew Knoll at the National Polymer Innovation Center (NPIC) in University of Akron with the assistance of XPS. We are also grateful to Dr Lingyan Li in National Center for Education and Research on Corrosion and Materials Performance (NCERAMP) at the University of Akron for the assistance of SEM analyses, and Mr Thomas J. Quick in Geosciences Department at the University of Akron for the assistance of XRD. The HRTEM test was taken at the (cryo) TEM facility at the Liquid Crystal Institute, Kent State University, supported by the Ohio Research Scholars Program Research Cluster on Surfaces in Advanced Materials. The authors thank Dr Min Gao for technical support with the TEM experiments.

References

- 1 G. J. Acres, Recent advances in fuel cell technology and its applications, *J. Power Sources*, 2001, **100**, 60–66.
- 2 N. Mahato, A. Banerjee, A. Gupta, S. Omar and K. Balani, Progress in material selection for solid oxide fuel cell technology: A review, *Prog. Mater. Sci.*, 2015, 72, 141–337.
- 3 L. Schlapbach, Technology: Hydrogen-fuelled vehicles, *Nature*, 2009, **460**, 809.
- 4 O. Z. Sharaf and M. F. Orhan, An overview of fuel cell technology: Fundamentals and applications, *Renewable Sustainable Energy Rev.*, 2014, **32**, 810–853.
- 5 S. McWhorter, C. Read, G. Ordaz and N. Stetson, Materials-based hydrogen storage: attributes for near-term, early market PEM fuel cells, *Curr. Opin. Solid State Mater. Sci.*, 2011, 15, 29–38.
- 6 U. B. Demirci and P. Miele, Chemical hydrogen storage: 'material' gravimetric capacity versus 'system'gravimetric capacity, *Energy Environ. Sci.*, 2011, 4, 3334–3341.
- 7 D. Teichmann, W. Arlt, P. Wasserscheid and R. Freymann, A future energy supply based on Liquid Organic Hydrogen Carriers (LOHC), *Energy Environ. Sci.*, 2011, 4, 2767–2773.
- 8 D. Teichmann, W. Arlt and P. Wasserscheid, Liquid Organic Hydrogen Carriers as an efficient vector for the

Paper

transport and storage of renewable energy, *Int. J. Hydrogen Energy*, 2012, **37**, 18118–18132.

- 9 U. Eberle, M. Felderhoff and F. Schueth, Chemical and physical solutions for hydrogen storage, *Angew. Chem., Int. Ed.*, 2009, **48**, 6608–6630.
- 10 N. Onishi, G. Laurenczy, M. Beller and Y. Himeda, Recent progress for reversible homogeneous catalytic hydrogen storage in formic acid and in methanol, *Coord. Chem. Rev.*, 2018, 373, 317–332.
- 11 L. E. Heim, H. Konnerth and M. H. Prechtl, Future perspectives for formaldehyde: pathways for reductive synthesis and energy storage, *Green Chem.*, 2017, 19, 2347–2355.
- 12 L. E. Heim, N. E. Schlörer, J.-H. Choi and M. H. Prechtl, Selective and mild hydrogen production using water and formaldehyde, *Nat. Commun.*, 2014, 5, 3621.
- 13 D. R. Palo, R. A. Dagle and J. D. Holladay, Methanol steam reforming for hydrogen production, *Chem. Rev.*, 2007, **107**, 3992–4021.
- 14 Y. Bi and G. Lu, Nano-Cu catalyze hydrogen production from formaldehyde solution at room temperature, *Int. J. Hydrogen Energy*, 2008, **33**, 2225–2232.
- 15 S. Enthaler, J. von Langermann and T. Schmidt, Carbon dioxide and formic acid-the couple for environmentalfriendly hydrogen storage?, *Energy Environ. Sci.*, 2010, 3, 1207–1217.
- 16 M. Brown and N. Parkyns, Progress in the partial oxidation of methane to methanol and formaldehyde, *Catal. Today*, 1991, 8, 305–335.
- 17 A. M. Bahmanpour, A. Hoadley and A. Tanksale, Critical review and exergy analysis of formaldehyde production processes, *Rev. Chem. Eng.*, 2014, **30**, 583–604.
- 18 P. Tijm, F. Waller and D. Brown, Methanol technology developments for the new millennium, *Appl. Catal., A*, 2001, 221, 275–282.
- 19 A. Álvarez, A. Bansode, A. Urakawa, A. V. Bavykina, T. A. Wezendonk, M. Makkee, J. Gascon and F. Kapteijn, Challenges in the greener production of formates/formic acid, methanol, and DME by heterogeneously catalyzed CO₂ hydrogenation processes, *Chem. Rev.*, 2017, 117, 9804–9838.
- 20 X. Tang, Y. Bai, A. Duong, M. T. Smith, L. Li and L. Zhang, Formaldehyde in China: production, consumption, exposure levels, and health effects, *Environ. Int.*, 2009, 35, 1210–1224.
- 21 H. R. Gerberich, G. C. Seaman and U. b. Staff, Formaldehyde, *Kirk-Othmer Encycl. Chem. Technol.*, 2000, 1–22.
- 22 A. M. Bahmanpour, A. Hoadley and A. Tanksale, Formaldehyde production via hydrogenation of carbon monoxide in the aqueous phase, *Green Chem.*, 2015, 17, 3500–3507.
- 23 A. M. Bahmanpour, A. Hoadley, S. H. Mushrif and A. Tanksale, Hydrogenation of carbon monoxide into formaldehyde in liquid media, ACS Sustainable Chem. Eng., 2016, 4, 3970–3977.
- 24 G. Sun, Z.-J. Zhao, R. Mu, S. Zha, L. Li, S. Chen, K. Zang, J. Luo, Z. Li and S. C. Purdy, Breaking the scaling relation-

- ship via thermally stable Pt/Cu single atom alloys for catalytic dehydrogenation, *Nat. Commun.*, 2018, 9, 4454.
- 25 E. M. Fernández, P. G. Moses, A. Toftelund, H. A. Hansen, J. I. Martínez, F. Abild-Pedersen, J. Kleis, B. Hinnemann, J. Rossmeisl and T. Bligaard, Scaling relationships for adsorption energies on transition metal oxide, sulfide, and nitride surfaces, *Angew. Chem., Int. Ed.*, 2008, 47, 4683–4686.
- 26 X. Hong, K. Chan, C. Tsai and J. K. Nørskov, How doped MoS₂ breaks transition-metal scaling relations for CO₂ electrochemical reduction, *ACS Catal.*, 2016, **6**, 4428–4437.
- 27 X. Feng, K. Jiang, S. Fan and M. W. Kanan, A direct grain-boundary-activity correlation for CO electroreduction on Cu nanoparticles, *ACS Central Sci.*, 2016, 2, 169–174.
- 28 C. W. Li, J. Ciston and M. W. Kanan, Electroreduction of carbon monoxide to liquid fuel on oxide-derived nanocrystalline copper, *Nature*, 2014, **508**, 504.
- 29 W. Luc, X. Fu, J. Shi, J.-J. Lv, M. Jouny, B. H. Ko, Y. Xu, Q. Tu, X. Hu and J. Wu, Two-dimensional copper nanosheets for electrochemical reduction of carbon monoxide to acetate, *Nat. Catal.*, 2019, 2, 423.
- 30 H. Zhang, X. Chang, J. G. Chen, W. A. Goddard, B. Xu, M.-J. Cheng and Q. Lu, Computational and experimental demonstrations of one-pot tandem catalysis for electrochemical carbon dioxide reduction to methane, *Nat. Commun.*, 2019, **10**, 3340.
- 31 Z. Ma and M. D. Porosoff, Development of tandem catalysts for CO₂ hydrogenation to olefins, *ACS Catal.*, 2019, **9**, 2639–2656.
- 32 J. Huang, M. Mensi, E. Oveisi, V. Mantella and R. Buonsanti, Structural Sensitivities in Bimetallic Catalysts for Electrochemical CO₂ Reduction Revealed by Ag–Cu Nanodimers, *J. Am. Chem. Soc.*, 2019, **141**, 2490–2499.
- 33 Y. Hori, A. Murata, R. Takahashi and S. Suzuki, Electroreduction of carbon monoxide to methane and ethylene at a copper electrode in aqueous solutions at ambient temperature and pressure, *J. Am. Chem. Soc.*, 1987, 109, 5022–5023.
- 34 X. Wang, J. F. de Araújo, W. Ju, A. Bagger, H. Schmies, S. Kühl, J. Rossmeisl and P. Strasser, Mechanistic reaction pathways of enhanced ethylene yields during electroreduction of $\rm CO_2\text{-}CO$ co-feeds on Cu and Cu-tandem electrocatalysts, *Nat. Nanotechnol.*, 2019, **14**, 1063–1070.
- 35 Y. Hori, A. Murata, R. Takahashi and S. Suzuki, Electrochemical reduction of carbon monoxide to hydrocarbons at various metal electrodes in aqueous solution, *Chem. Lett.*, 1987, **16**, 1665–1668.
- 36 H. Hansen, C. Shi, A. Lausche, A. Peterson and J. Nørskov, Bifunctional Alloys for the Electroreduction of CO₂ and CO, *Phys. Chem. Chem. Phys.*, 2016, **18**, 9194–9201.
- 37 E. Bertheussen, A. Verdaguer-Casadevall, D. Ravasio, J. H. Montoya, D. B. Trimarco, C. Roy, S. Meier, J. Wendland, J. K. Nørskov and I. E. Stephens, Acetaldehyde as an intermediate in the electroreduction of carbon monoxide to ethanol on oxide-derived copper, Angew. Chem. Int. Ed., 2016, 55, 1450–1454.
- 38 K. J. P. Schouten, E. Pérez Gallent and M. T. M. Kroper, Structure sensitivity of the electrochemical reduction of

- carbon monoxide on copper single crystals, ACS Catal., 2013, 3, 1292–1295.
- 39 M. Jouny, W. Luc and F. Jiao, High-rate electroreduction of carbon monoxide to multi-carbon products, *Nat. Catal.*, 2018, 1, 748.
- 40 T.-Y. An, S. Surendran, H. Kim, W.-S. Choe, J. K. Kim and U. Sim, A polydopamine-mediated biomimetic facile synthesis of molybdenum carbide-phosphide nanodots encapsulated in carbon shell for electrochemical hydrogen evolution reaction with long-term durability, *Composites, Part B*, 2019, 175, 107071.
- 41 M. S. Duyar, C. Tsai, J. L. Snider, J. A. Singh, A. Gallo, J. S. Yoo, A. J. Medford, F. Abild-Pedersen, F. Studt and J. Kibsgaard, A Highly Active Molybdenum Phosphide Catalyst for Methanol Synthesis from CO and CO₂, *Angew. Chem., Int. Ed.*, 2018, 130, 15265–15270.
- 42 P.-w. Wu, C.-c. Chang and S.-s. Chou, Determination of formaldehyde in cosmetics by HPLC method and acetylacetone method, *J. Food Drug Anal.*, 2003, **11**, 8–15.

- 43 P. Giannozzi, S. Baroni, N. Bonini, M. Calandra, R. Car, C. Cavazzoni, D. Ceresoli, G. L. Chiarotti, M. Cococcioni and I. Dabo, QUANTUM ESPRESSO: a modular and opensource software project for quantum simulations of materials, J. Phys.: Condens. Matter, 2009, 21, 395502.
- 44 A. Dal Corso, Pseudopotentials, periodic table: From H to Pu, *Comput. Mater. Sci.*, 2014, **95**, 337–350.
- 45 P. Xiao, M. A. Sk, L. Thia, X. Ge, R. J. Lim, J.-Y. Wang, K. H. Lim and X. Wang, Molybdenum phosphide as an efficient electrocatalyst for the hydrogen evolution reaction, *Energy Environ. Sci.*, 2014, 7, 2624–2629.
- 46 Z. Zhou, L. Wei, Y. Wang, H. E. Karahan, Z. Chen, Y. Lei, X. Chen, S. Zhai, X. Liao and Y. Chen, Hydrogen evolution reaction activity of nickel phosphide is highly sensitive to electrolyte pH, *J. Mater. Chem. A*, 2017, 5, 20390–20397.
- 47 M. Wu, P. K. Shen, Z. Wei, S. Song and M. Nie, High activity PtPd-WC/C electrocatalyst for hydrogen evolution reaction, *J. Power Sources*, 2007, 166, 310–316.